



The December 22, 2018 Anak Krakatau, Indonesia, Landslide and Tsunami: Preliminary Modeling Results

ALEXANDRE PARIS,^{1,3} PHILIPPE HEINRICH,¹ RAPHAËL PARIS,² and STÉPHANE ABADIE³

Abstract—On the evening of December 22, 2018, the coasts of the Sunda Strait, Indonesia, were hit by a tsunami generated by the collapse of a part of the Anak Krakatau volcano. Hundreds of people were killed, thousands were injured and displaced. This paper presents a preliminary modeling of the volcano flank collapse and the tsunami generated based on the results of a 2D depth-averaged coupled model involving a granular rheology and a Coulomb friction for the slide description and dispersive effects for the water flow part. With a reconstructed total volume (subaerial and submarine) of the landslide of 150 million m³ inferred from pre and post-collapse satellite and aerial images, the comparison of the simulated water waves with the observations (tide gauges located all around the strait, photographs and field surveys) is satisfactory. Due to the lack of information for the submarine part of the landslide, the reconstructed submarine slope is assumed to be approximately constant. A significant time delay on the results and particularly in the Bandar Lampung Bay could be attributed to imprecisions of bathymetric data. The sensitivity to the basal friction and to dispersive effects is analyzed through numerical tests. Results show that the influence of the basal friction angle on the simulated wave heights decreases with distance and that a value of 2° gives consistent results with the observations. The dispersive effects are assessed by comparing water waves simulated by a shallow water model and a Boussinesq model. Simulations with frequency dispersion produce longer wave periods and smaller wave amplitudes in the Sunda Strait and particularly in deep waters.

Keywords: Tsunami, landslide, Anak Krakatau, simulation.

1. Introduction

Landslide tsunamis are not very well known to the general public, although they are quite common and devastating. This phenomenon can happen wherever weakened volumes of rocks or sediments lie, i.e. in deltas, coastal cliffs, rivers, fjords and lakes (Masson et al. 2006). As the velocity of the terrain deformation due to a landslide can reach very high values (up to 100 m.s⁻¹ according to Satake et al. (2002)), the tsunami energy may be initially of the same order as that generated by a major earthquake (Okal and Synolakis 2003), but the generated amplitudes generally decrease quickly and the tsunami effects are local.

One of the largest landslide tsunamis may probably be the Storegga slide, off Norway, with its volume between 2400 and 3200 km³, 8200 years ago (Hafstad et al. 2004; Bondevik et al. 2005). Another famous case is the 1958 Lituya Bay landslide-generated mega-tsunami (Miller 1960). After a 8.3-magnitude earthquake, a volume of 30.6 million m³ collapsed in Gilbert Inlet, generating a tsunami which run-up height reached 524 m on the opposite side (Fritz et al. 2009).

Until now, one of the deadliest recent landslide tsunamis is the Papua New Guinea one, 1998, during which over 2100 people died after a 4 km³ landslide collapsed at a depth of 550 m, generating a tsunami with run-up heights up to 15 m (Heinrich et al. 2001a; Synolakis et al. 2002). More recently, the 2014 Tangjiaxi, China (0.16 million m³, 3 deaths, 9 people missing and 11 injured (Huang et al. 2017)), the 2017 Karrat Fjord, Greenland (50 million m³, 4 people killed (Paris et al. 2019)) events and now the 2018 Anak Krakatau, Indonesia collapse remind us of

¹ CEA, DAM, DIF, 91297 Arpajon Cedex, France. E-mail: alexandre.antoine.paris@gmail.com

² Université Clermont Auvergne, CNRS, IRD, OPGC, Laboratoire Magmas et Volcans, 63000 Clermont-Ferrand, France.

³ Université de Pau et des Pays de l'Adour, E2S UPPA, SIAME, Anglet, France.

the threat landslide tsunamis represent, even if their volume appear relatively small compared to historical events such as Ritter Island in 1888 (5 km^3) (Cooke 1981; Johnson 1987)) and Oshima–Oshima in 1741 (2.4 km^3) (Satake and Kato 2001).

A possible way to better understand a physical phenomenon is to use numerical modeling. A review of landslide-generated tsunami models can be found in Heidarzadeh et al. (2014) and Yavari-Ramshe and Ataie-Ashtiani (2016). Two approaches are used to simulate landslide-generated tsunamis: simulate the tsunami propagation considering the bottom deformation due to the landslide as a boundary condition for the water surface elevation or simulate both the landslide and the tsunami in a single model. In the first category, the landslide movement is reproduced as a bathymetry deformation in time (see Harbitz (1992), Grilli and Watts (2005) or Tappin et al. (2008)). In the second category, the landslide is modeled together with the free surface using a rheology law. Among them we can find Newtonian fluid approaches as in the numerical experiments of Fine et al. (2003), or in the modeling of the 1979 Nice events (Assier-Rzadkiewicz et al. 2000), or in the Franz et al.'s (2015) study of the 2006 Nicolet, Québec, Canada, landslide. Non-Newtonian models such as the Bingham model of Skvortsov and Bornhold (2007) or the BING model (e.g. the modeling of the 1888 Brattora, Norway, landslide tsunami (L'Heureux et al. 2011) or the 2014 submarine landslide at Statland, Norway (Glimsdal et al. 2016)) can also be used. Finally, landslides rheologies can be modeled as granular flows, as in the study of Reunion Island landslide-tsunamis by Kelfoun et al. (2010) or the Güímar debris avalanche simulation of Giachetti et al. (2011).

Landslides are mostly simulated using 2D depth-averaged (2DH) models, although more complex and time-consuming 3D computations may be envisaged (Løvholt et al. 2008; Abadie et al. 2012; Horrillo et al. 2013). Nevertheless, they are generally spatially restricted to the landslide and wave generation area. Tsunami propagation can be realized in 2DH using shallow water equations (Jiang and LeBlond 1992; Harbitz et al. 1993) or Boussinesq equations (Tappin et al. 2014; Harbitz et al. 2014; Grilli et al. 2015). Here, we use the 2D depth-integrated model

AVALANCHE (Heinrich and Piatanesi 2000; Hébert et al. 2002; Le Friant et al. 2003) that has been successfully employed to simulate subaerial or submarine landslides (Rodriguez et al. 2013; Poupartdin et al. 2017; Paris et al. 2019), considering the landslide as a granular flow following a Coulomb frictional law and using shallow water or Boussinesq equations.

On December 22, 2018 at 13:50 UTC (20:50 local time) the southwestern flank of Anak Krakatau volcano (Sunda Strait, Indonesia) collapsed to the sea and generated a tsunami that devastated the coasts of Java and Sumatra, killing more than 430 people and damaging thousands of houses and boats, as reported by BNPB (Badan Nasional Penanggulangan Bencana¹). Human casualties and material losses were recorded all around the Sunda Strait, on the islands of Java and Sumatra, with run-up heights reaching up to 14 m (TDMRC 2019). A summary of the available observations data is provided in Sect. 3. This Anak Krakatau event was recently studied by Grilli et al. (2019), using the 3D model NHWAVE (Ma et al. 2012, 2015; Kirby et al. 2016) for the landslide simulation and the tsunami generation, then the 2D model FUNWAVE-TVD (Shi et al. 2012) for the tsunami propagation. It was also simulated by Heidarzadeh et al. (2020) using the COMCOT model (Cornell Multi-grid Coupled Tsunami Model (Liu et al. 1998; Wang and Liu 2006)) and an initial sea surface elevation as the landslide source. We present a comparison between water heights of the two latter mentioned studies and our simulation.

In this paper, the landslide-generated water waves are calculated by AVALANCHE and compared with available tsunami observations around Sunda Strait (tide gauge records, wave heights, and flow depths, inundation heights and run-up heights reported from three field surveys). The influence of the rheology on water wave heights is discussed using different basal friction angle values and finally the dispersive effects are assessed through numerical tests comparing a shallow water to a Boussinesq model.

¹ <https://bnpb.go.id/volume-tubuh-gunung-anak-karakatau-berkurang-jumlah-korban-tsunami-bertambah>, last accessed 10 september 2019.

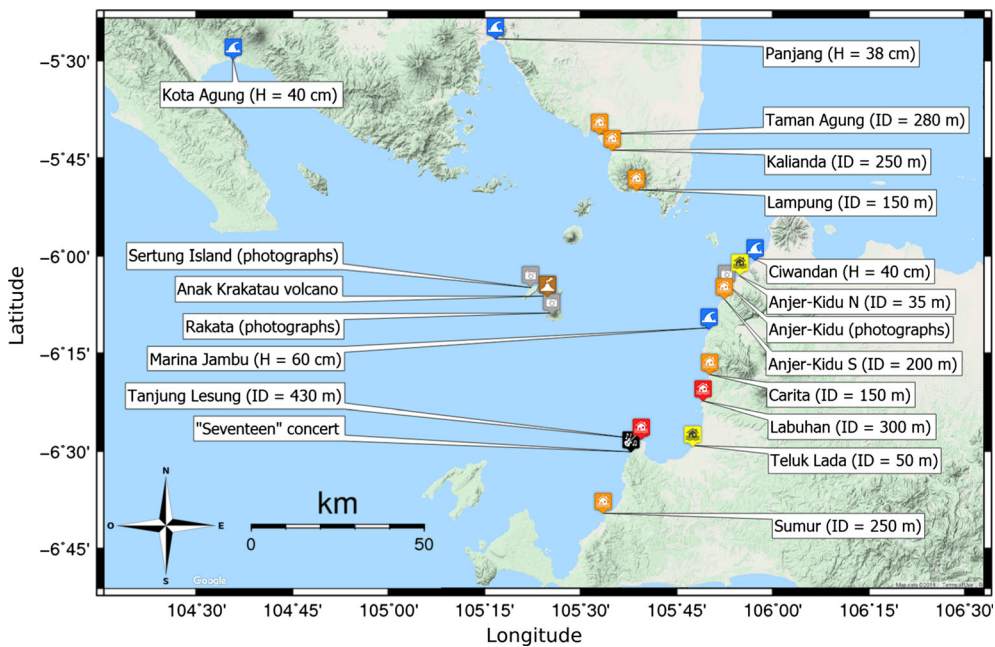


Figure 1

Location map of Anak Krakatau volcano in the Sunda Strait (brown volcano icon) and of the different observations of the event: inundation distance *ID* (less than 100 m in yellow, between 100 and 300 m in orange and more than 300 m in red), recorded height *H* at tide gauges (blue icons) and photographs (grey icons)

2. Geological Setting

The Krakatau volcanic complex is a group of islands that lies in the middle of the Sunda Strait, between Java and Sumatra. The tectonic setting of the strait is characterized by an extensional regime that formed different grabens at the southeastern end of the Sumatra fault zone (Harjono et al. 1991; Susilohadi et al. 2009). With a water depth not exceeding 200 m, the eastern part of the strait is relatively shallow, compared with the 1000 m deep Semangko graben to the west (see Figure 2 in Susilohadi et al. (2009)).

Krakatau is the only active volcano of a south-southwest to north-northeast volcanic line that extends across the strait from Ujung Kulon in western Java to Rajabasa in eastern Sumatra (Nishimura et al. 1986). The 1883 caldera-forming eruption completely reshaped the morphology of the Krakatau volcanic complex (e.g. Simkin and Fiske (1983)), and the present-day active edifice Anak Krakatau ('child of Krakatau' in Indonesian) was built on the steep

northeast wall of the submarine caldera that was formed during the 1883 eruption (Deplus et al. 1995). The $5 \times 4 \text{ km}^2$ large rectangular caldera is characterized by a flat bottom of 200–240 m deep. The location of Anak Krakatau on the northeast rim of this steep-sided submarine basin led several authors to question its stability (Camus et al. 1987; Deplus et al. 1995; Giachetti et al. 2012). During this 1883 eruption, a tsunami was generated, reaching 15 up to 40 m run-up heights in the Sunda Strait (Nomanbhoy and Satake 1995; Choi et al. 2003) and killing more than 35,000 people (Sigurdsson et al. 1991).

Anak Krakatau first emerged from the sea in January 1928 (Stehn 1929). From 1928 to 1959 phreatomagmatic activity progressively formed a 1.7 km large, 150 m high tuff-ring (Sudradjat 1982). In 1960, eruptive activity shifted to a Strombolian style, thus building a new cone on the SW flank of the initial tuff-ring. During the last 60 years, recurrent lava flows and pyroclastic fall deposits contributed to the growth of Anak Krakatau Island, and the cone was 350 m high before its collapse in December

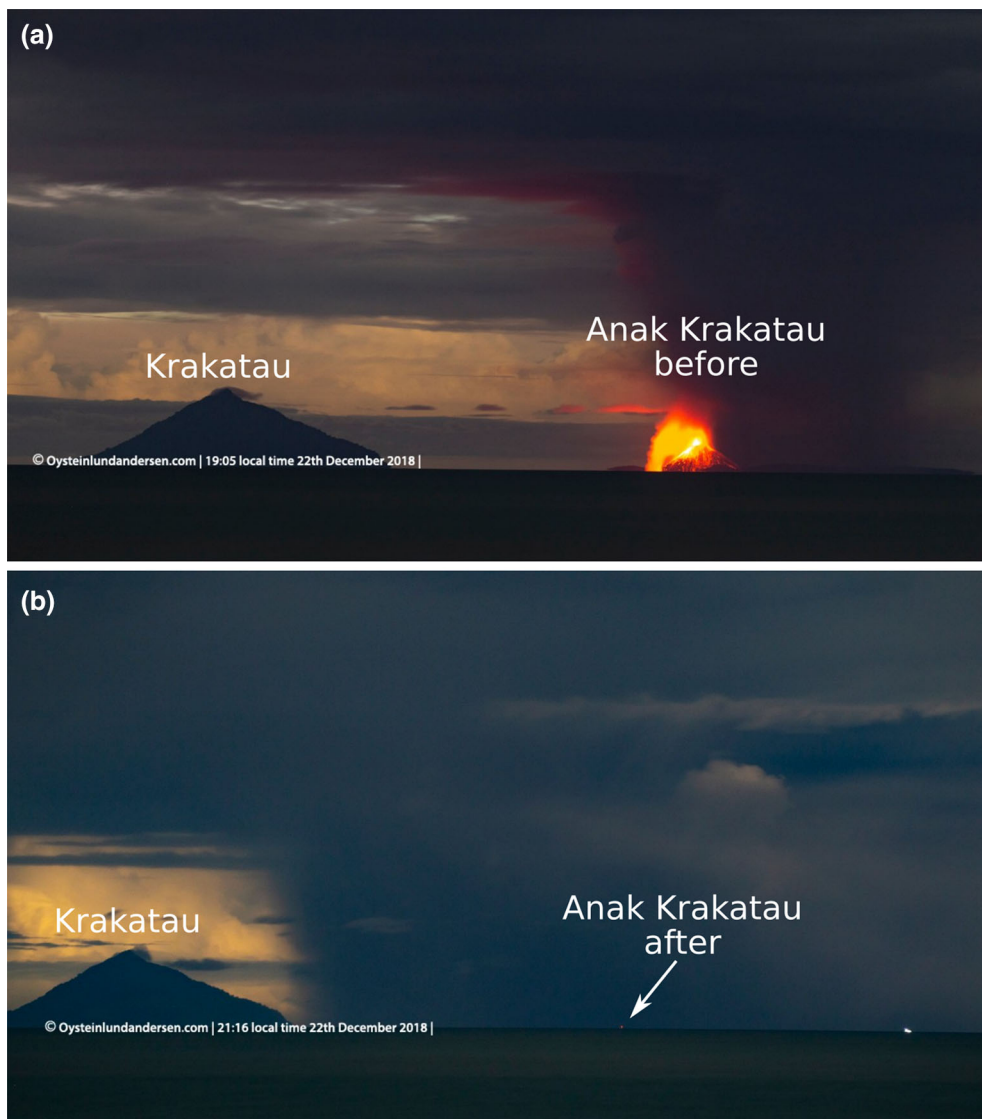


Figure 2

Photographs taken in Anjer-Kidu, 50 km east of the volcano, **a** before the landslide at 19:05 local time and **b** after the landslide at 21:16 local time (<https://www.oysteinlundandersen.com/krakatau-volcano-witnessing-the-eruption-tsunami-22december2018/>)

2018. Photographs captured from the coast of Java² confirmed that the cone had grew by almost 100 m between July 2016 and December 2018. There are many coastal resorts, harbors and cities within a radius of 60 km around the volcano [e.g. Kalianda in Sumatra, Anjer, Labuhan and Sumur in Java (Fig. 1)].

² <https://www.oysteinlundandersen.com/krakatau-volcano-witnessing-the-eruption-tsunami-22december2018/>.

3. Anatomy of the Event

Before any satellite revealed the effects of the ongoing volcanic eruption and collapse, photographs captured by Øystein Lund Andersen in Anjer-Kidu (western coast of Java, 50 km east of Krakatau volcano) show a strong strombolian activity (Fig. 2a), followed by a phase of ash emission that blurred the entire volcano (Fig. 2b). The collapse was recorded on a seismic signal at 20:55 local time, i.e. 13:55

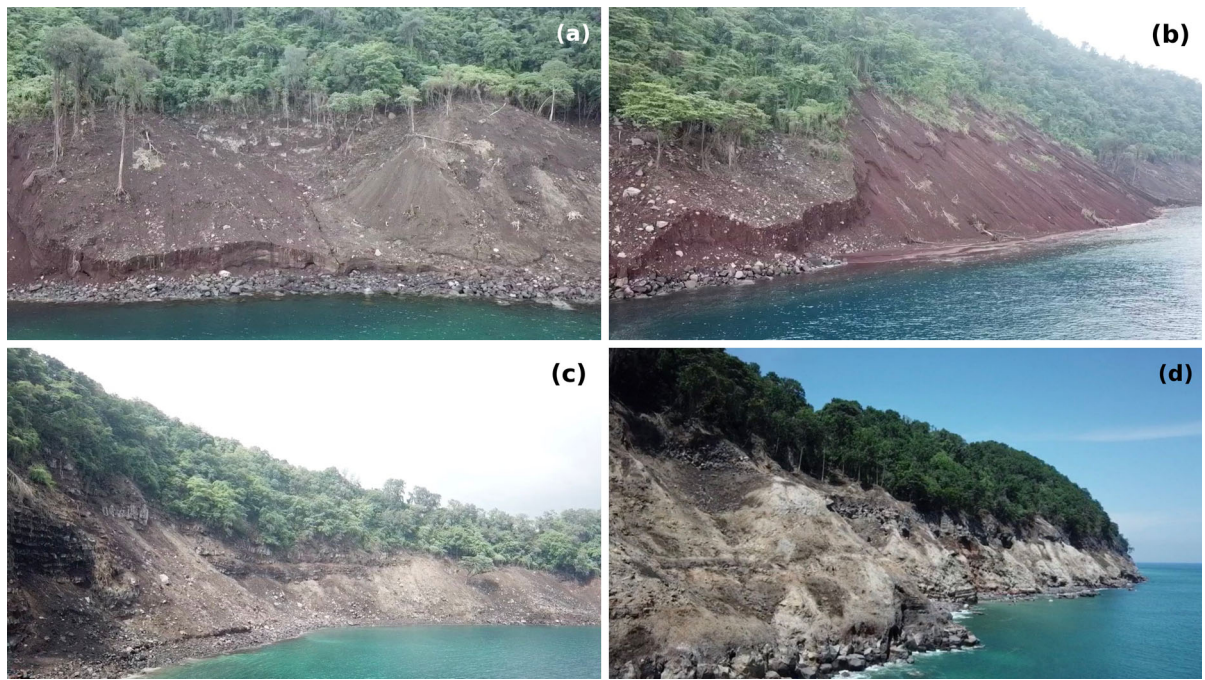


Figure 3

Photographs of inundation effects in the near-field on **a, b, c** Rakata Island and **d** Sertung Island (Fig. 1), close to the Anak Krakatau volcano (James Reynolds @EarthUncutTV on Twitter: <https://twitter.com/earthuncutv/status/1083305942228160513>). The base of trees is estimated to be now 25 to 30 m above sea level

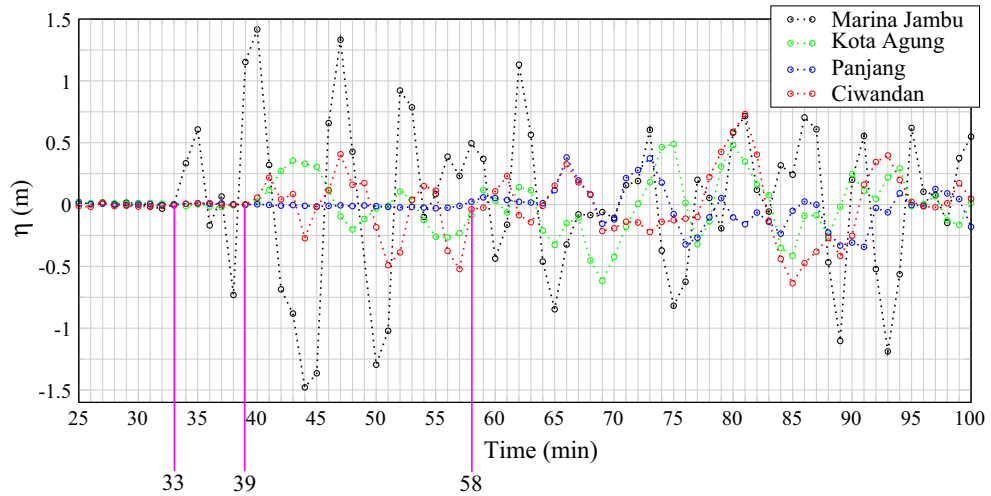


Figure 4

Time series of surface elevation recorded by tide gauges at Marina Jambu (black), Ciwandan (red), Kota Agung (green) and Panjang (blue) tide gauges (see Fig. 9 for locations). Pink lines mark the arrival times at each tide gauges. The arrival times at Kota Agung and Ciwandan are identical

UTC (Walter et al. 2019). The flank collapse which removed 93.8 million m^3 of subaerial volcanic rocks from the western side of the volcano (Gouhier and Paris 2019) followed a period of 6 months of volcanic

activity and rapid growth of the volcanic cone (Gouhier and Paris 2019; Walter et al. 2019).

Local effects of the tsunami generated by the flank collapse are visible on Rakata Island (Fig. 3a–c)

Table 1
Summary of results sorted by arrival times

| Gauges location | Coordinates (longitude, latitude) | Depth (m) | Travel time (min) | | | Wave Height (cm) | |
|--------------------|-----------------------------------|-----------|-------------------------|-------|------|------------------|---------|
| | | | Giachetti et al. (2012) | Comp. | Rec. | Comp. | Rec. |
| 1-Near the volcano | 105.31376, – 6.14967 | 100 | ø | 5 | ø | 560 | ø |
| 2-Tanjung Lesung | 105.64894, – 6.47980 | 1.5 | 28 | 29 | ø | 170 | 100–200 |
| 3-Marina Jambu | 105.84263, – 6.18953 | 1.8 | 33 | 34 | 33 | 75 | 60 |
| 4-Ciwandan | 105.95513, – 6.01441 | 1.1 | 42 | 42 | 39 | 22 | 20 |
| 6-Kota Agung | 104.62044, – 5.50120 | 1.0 | ø | 45 | 39 | 33 | 35 |
| 5-Kalianda | 105.55701, – 5.70134 | 2.9 | 47 | 49 | ø | 120 | ø |
| 7-Panjang | 105.29036, – 5.44579 | 1.3 | 68 | 66 | 58 | 20 | 37 |

Computed (*Comp.*) results are compared with recorded (*Rec.*) data and Giachetti et al.'s (2012) results. Gauges number refer to Fig. 9

and Sertung Island (Fig. 3d). Taking into account the trimline, the run-up height is estimated to 25 up to 30 m on Rakata and Sertung islands, located respectively 4 km south and 3 km north-northwest of Anak Krakatau Island.

About 33 min after the collapse, the tsunami was recorded at Marina Jambu, Banten, east of the volcano on Java Island (Fig. 1), with a first water wave height of 60 cm and 6 min later a 20 cm high wave was recorded at Ciwandan, north of Marina Jambu (Fig. 4). At the same time, on Sumatra Island, a tide gauge located at Kota Agung, northwest of the Anak Krakatau, recorded a wave height of 35 cm. Finally, 58 min after the collapse, the tsunami was recorded in the Bandar Lampung Bay at Panjang, north of the volcano, with a wave height of 37 cm. Note that for the two locations of Marina Jambu and Ciwandan, on Java Island, the first wave is not the highest one. In both cases, the second wave height is twice or more the first one and reached 140 cm at Marina Jambu, and 40 cm at Ciwandan.

Thanks to the work of the Copernicus program³, preliminary summary maps about the consequences of the tsunami were made available. These maps give an idea about inundation distances and damages on houses. On Java Island, the most affected areas are Labuhan, with up to 300 m of inundation distance and Tanjung Lesung (see Fig. 1 for locations), where the water entered up to 430 m inland. South of Tanjung Lesung, a YouTube video⁴ shows a water wave, that

can be estimated between 1 and 2 m high, destroying a concert stage. Elsewhere, the inundation distances reached approximately 35 m north of Anjer-Kidu, 50 m at Teluk Lada, 170 m at Carita, 200 m south of Anjer-Kidu, and 250 m in Sumur. On Sumatra Island, the water penetrated the land up to 150 m at Lampung, 250 m at Kalianda and 280 m at Taman Agung. Locations, inundation distances and recorded water heights are summarized in Fig. 1 and Table 1.

Finally, the field surveys conducted by the KKP (Kementerian Kelautan dan Perikanan, Ministry of Marine Affairs and Fisheries) south of Tanjung Lesung and between Labuhan and Anjer-Kidu (Muhari et al. 2019), the BMKG (Badan Meteorologi, Klimatologi, dan Geofisika) at Tanjung Lesung and Carita, and the Tsunami and Disaster Mitigation Research Center of Syiah Kuala University confirmed that the areas of Tanjung Lesung, Labuhan, Carita and Anjer-Kidu on Java Island and Kalianda on Sumatra Island were among the most impacted, with destroyed brick walls and boulder(s) displaced (TDMRC 2019). These different field surveys confirmed that the waves penetrated up to 300 m inland at Tanjung Lesung (run-up height of 5 m asl), 170 m at Carita (run-up height of 6.2 m asl) and 330 m at Sakarame, north Carita (run-up height of 4.6 m asl). A local run-up height of 13.5 m asl for an inundation distance of 125 m was measured in a location between Tanjung Lesung and Sumur. Another remarkable run-up height of 12.5 m was measured at Cipenu Beach by Takabatake et al. (2019). The locations of the places studied by these field surveys are listed in Tables 2 and 3.

³ <https://emergency.copernicus.eu/mapping/list-of-components/EMSR335>.

⁴ <https://www.youtube.com/watch?v=2ERXCR86GU4>.

Table 2

Computed water heights (W.H.) (m) at the shoreline compared with flow depths (F.D.), inundation heights (I.H.) and run-up heights (R.H.) identified by the Takabatake et al. (2019) and BMKG surveys

| Places | Coordinates (longitude, latitude) | W.H. (m) computed | Takabatake et al.'s (2019) Survey | | |
|-----------------|-----------------------------------|-------------------|-----------------------------------|-------------|-------------|
| | | | F.D. (m) | I.H. (m) | R.H. (m) |
| Sinar Agung | 105.10208, - 5.77083 | 0.4 | | 2.35 (10) | |
| Sinar Agung | 105.10128, - 5.77061 | 0.4 | | 1.58 (20) | |
| Bandung Jaya | 105.10533, - 5.77611 | 0.4 | | 0.81 (0) | |
| Bandung Jaya | 105.10936, - 5.77353 | 0.5 | | 1.74 (36) | |
| Selesung | 105.29231, - 5.80242 | 0.4 | | 3.38 (15) | |
| Selesung | 105.29231, - 5.80261 | 0.4 | | 3.38 (31) | |
| Central Waymuli | 105.63419, - 5.83739 | 0.6 | | | 5.04 (75) |
| East Waymuli | 105.64164, - 5.83558 | 1.2 | | | 3.97 (79) |
| Kunjir | 105.65161, - 5.83592 | 0.9 | | 4.21 (76) | |
| Kahai Beach | 105.66814, - 5.83789 | 2.3 | | 6.83 (22) | |
| Tangkolo | 105.82944, - 6.26461 | 1.3 | | 1.01 (198) | |
| Lantera | 105.82314, - 6.37628 | 1.9 | | 3.36 (39) | |
| Cipenu Beach | 105.64139, - 6.50536 | 2.7 | | | 12.58 (185) |
| Cipenu Beach | 105.64083, - 6.50417 | 2.7 | | 11.28 (85) | |
| Cipenu Beach | 105.64108, - 6.50419 | 2.7 | | 10.17 (114) | |
| Tanjung Jaya | 105.62436, - 6.54508 | 2.5 | | 5.39 (170) | |
| Babakanciberber | 105.61847, - 6.60589 | 0.9 | | | 2.55 (48) |

| Places | Coordinates (longitude, latitude) | W.H. (m) computed | BMKG Survey | | |
|----------------|-----------------------------------|-------------------|--------------------|--------------------|----------|
| | | | F.D. (m) | I.H. (m) | R.H. (m) |
| Tanjung Lesung | 105.65463, - 6.48015 | 3 | | 5.06 (60) [303.31] | |
| Tanjung Lesung | 105.65453, - 6.48010 | 3 | 4.23 (50) [303.31] | | |
| Mutiara Carita | 105.83200, - 6.31613 | 3 | | 3.05 (24) [170.28] | |
| Mutiara Carita | 105.83200, - 6.31644 | 3 | 2.9 (55) [170.28] | | |
| Mutiara Carita | 105.83018, - 6.31634 | 2.4 | | 5.08 (14) [170.28] | |
| Mutiara Carita | 105.82907, - 6.31728 | 3 | | 5.04 (10) [170.28] | |
| Mutiara Carita | 105.82828, - 6.31876 | 3.4 | | 5.64 (12) [170.28] | |
| Mutiara Carita | 105.82828, - 6.31996 | 4.3 | | 6.22 (14) [170.28] | |
| Carita Lagon | 105.82678, - 6.28562 | 2.5 | 3.05 (18) [95.90] | | |

Values in parenthesis are the distances from the shoreline. Values in brackets are the maximum inundation distances measured by the different team surveys

4. Methods

4.1. Landslide Model

In the code AVALANCHE (Heinrich et al. 2001b; Paris et al. 2019) the flank collapse is modeled using the one-phase grain-flow model of Savage and Hutter (1989) and a Coulomb basal friction. The equations of conservation of mass and momentum are solved in a (x', y') coordinate system linked to the topography (Fig. 5):

$$\frac{\partial h_s}{\partial t} + \frac{\partial}{\partial x'}(h_s u_s) + \frac{\partial}{\partial y'}(h_s v_s) = 0; \quad (1)$$

$$\frac{\partial}{\partial t}(h_s u_s) + \frac{\partial}{\partial x'}(h_s u_s^2) + \frac{\partial}{\partial y'}(h_s u_s v_s) = -\frac{1}{2}\kappa \frac{\partial}{\partial x'}(gh_s^2 \cos \theta) + \kappa g h_s \sin \theta_x + F_{x'}; \quad (2)$$

$$\frac{\partial}{\partial t}(h_s v_s) + \frac{\partial}{\partial x'}(h_s v_s u_s) + \frac{\partial}{\partial y'}(h_s v_s^2) = -\frac{1}{2}\kappa \frac{\partial}{\partial y'}(gh_s^2 \cos \theta) + \kappa g h_s \sin \theta_y + F_{y'} \quad (3)$$

where h_s is the slide's thickness in a direction perpendicular to the slope, $\mathbf{u} = (\mathbf{u}_s, \mathbf{v}_s)$ the depth-averaged velocity vector parallel to the slope, $\kappa = 1 - \rho_w/\rho_s$ where ρ_w and ρ_s are the water and rock densities with a ratio $\rho_s/\rho_w = 1.5$ (for the subaerial

Table 3

Computed water heights (W.H.) (m) at the shoreline compared with flow depths (F.D.), inundation heights (I.H.) and run-up heights (R.H.) identified by the KKP survey

| Places | Coordinates (longitude, latitude) | W.H. (m) computed | KKP survey | | |
|---------------|-----------------------------------|-------------------|-------------|----------|---------------------|
| | | | F.D. (m) | I.H. (m) | R.H. (m) |
| Karang Suraga | 105.85470, - 6.15110 | 0.8 | | | 3.74 (31) [84.47] |
| Karang Suraga | 105.84969, - 6.16902 | 0.8 | | | 3.29 (51) [57.76] |
| Karang Suraga | 105.84697, - 6.17453 | 0.9 | 0.81 (26) | | |
| Karang Suraga | 105.84747, - 6.17476 | 0.9 | | | 4.54 (85) [94.64] |
| Bulakan | 105.83830, - 6.19698 | 0.8 | 0.63 (- 21) | | |
| Bulakan | 105.83619, - 6.20232 | 1.2 | | | 5.8 (90) [124.13] |
| Umbul Tanjung | 105.82577, - 6.23888 | 1.8 | | | 5.34 (64) [68.8] |
| Sukarame | 105.82887, - 6.26210 | 1.2 | 3.2 (15) | | 4.57 (15) [330] |
| Sukarame | 105.82698, - 6.27677 | 1.6 | | | 3.45 (105) [158.92] |
| Sukarame | 105.82700, - 6.27700 | 1.6 | 1.14 (94) | | |
| Tanjung Jaya | 105.65939, - 6.48078 | 3 | | | 7.07 (74) [158.84] |
| Tanjung Jaya | 105.65935, - 6.48047 | 3 | 1.65 (64) | | |
| Tanjung Jaya | 105.65940, - 6.48005 | 3 | 3.1 (18) | | |
| Tanjung Jaya | 105.65817, - 6.47995 | 3 | 1.23 (37) | | |
| Tanjung Jaya | 105.65817, - 6.48033 | 3 | 0.77 (77) | | |
| Cipenu Beach | 105.64078, - 6.50363 | 2.7 | 1.3 (90) | | |
| Cipenu Beach | 105.64101, - 6.50466 | 2.7 | 2.24 (117) | | |
| Cipenu Beach | 105.64165, - 6.50461 | 2.7 | 1.51 (186) | | |
| Cipenu Beach | 105.63815, - 6.50781 | 2.1 | | | 8.51 (42) [66.59] |
| Pantai Legon | 105.63335, - 6.51699 | 2.3 | | | 13.49 (42) [124.58] |
| Tanjung Jaya | 105.62888, - 6.52415 | 2.6 | | | 10.94 (97) [159.42] |
| Tanjung Jaya | 105.62673, - 6.5296 | 2.8 | | | 13.2 (154) [121.83] |
| Pantai Batu | 105.62356, - 6.54209 | 1.2 | 1.54 (62) | | |
| Banyuasih | 105.62223, - 6.55211 | 2.5 | 1.82 (63) | | |
| Banyuasih | 105.61664, - 6.56774 | 1.8 | 5.40 (11) | | |
| Banyuasih | 105.61785, - 6.56787 | 1.8 | 1.25 (144) | | |
| Banyuasih | 105.61800, - 6.56839 | 1.8 | 0.43 (176) | | |

Values in parenthesis are the distances from the shoreline. Values in brackets are the maximum inundation distances measured by the different team surveys

part of the slide, κ is equal to 1), $\theta(x, y)$ the local steepest slope angle, θ_x and θ_y the slope angles along the x and y axes respectively, and $\mathbf{F} = -\kappa \mathbf{g} \mathbf{h}_s \cos(\theta) \tan(\phi) \mathbf{u} / \|\mathbf{u}\|$ the friction forces, where ϕ is the friction angle of the sliding materials. Curvature terms representing the effects of coordinate transformations (Savage and Hutter 1991) are considered as second-order terms in this paper. In this set of equations, water acts on the slide only through a buoyancy term and any drag contribution is neglected.

The basal friction angle is adjusted through a sensitivity study to fit with the observed water waves at the four tide gauges that recorded the tsunami. Values of 1, 2, 5 and 10° were tested and results were analyzed in the near-field (Gauge 1, Fig. 6a) and in the far-field (Gauge 3, Fig. 6b and Gauge 6, Fig. 6c).

Gauges locations are presented in Fig. 9 and listed in Table 1.

4.2. Tsunami Model

As in Paris et al. (2019), tsunami generation is modeled by solving shallow water equations (Eqs. 4, 5, 6) during 80 s after the landslide triggering. Beyond 80 s, Boussinesq equations Eqs. (7, 8, 9) are solved in order to take into account any possible dispersive effects during the propagation. The shallow water equations solved by AVALANCHE are written as:

$$\frac{\partial \eta}{\partial t} + \frac{\partial(hu)}{\partial x} + \frac{\partial(hv)}{\partial y} = - \frac{\partial d}{\partial t}; \quad (4)$$

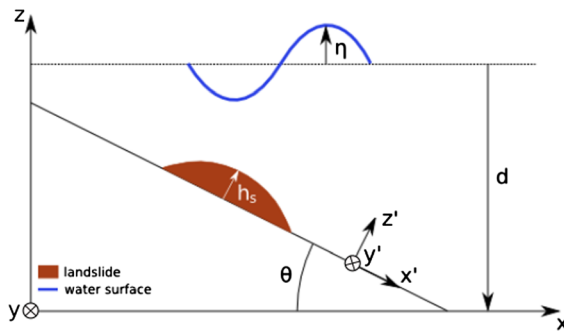


Figure 5

Definition of parameters used in the AVALANCHE model, with h_s the slide's thickness, η the surface elevation, d the depth and θ the local steepest slope angle

$$\frac{\partial u}{\partial t} + u \frac{\partial u}{\partial x} + v \frac{\partial u}{\partial y} = -g \frac{\partial \eta}{\partial x} + F_x; \quad (5)$$

$$\frac{\partial v}{\partial t} + u \frac{\partial v}{\partial x} + v \frac{\partial v}{\partial y} = -g \frac{\partial \eta}{\partial y} + F_y \quad (6)$$

where η is the surface elevation, $h = \eta + d$ the water column height, d is the depth, u and v the depth-averaged velocities along the x and y axes respectively and F_x and F_y the friction and Coriolis forces, which are assumed to be negligible in our modeling.

Following Løvholt et al. (2008), the Boussinesq equations read:

$$\frac{\partial \eta}{\partial t} + \frac{\partial(hu)}{\partial x} + \frac{\partial(hv)}{\partial y} = -\frac{\partial d}{\partial t}; \quad (7)$$

$$\begin{aligned} \frac{\partial u}{\partial t} + u \frac{\partial u}{\partial x} + v \frac{\partial u}{\partial y} &= -g \frac{\partial \eta}{\partial x} + \frac{d^3}{3} \left[\frac{\partial^2 u_t}{\partial x^2} + \frac{\partial^2 v_t}{\partial x \partial y} \right] \\ &+ \frac{d}{2} \left[u_t \frac{\partial^2 d}{\partial x^2} + u_t \frac{\partial^2 d}{\partial x \partial y} \right] + d \frac{\partial d}{\partial x} \frac{\partial u_t}{\partial x} \\ &+ \frac{d}{2} \left[\frac{\partial d}{\partial x} \frac{\partial v_t}{\partial y} + \frac{\partial d}{\partial y} \frac{\partial v_t}{\partial x} \right] + F_x; \end{aligned} \quad (8)$$

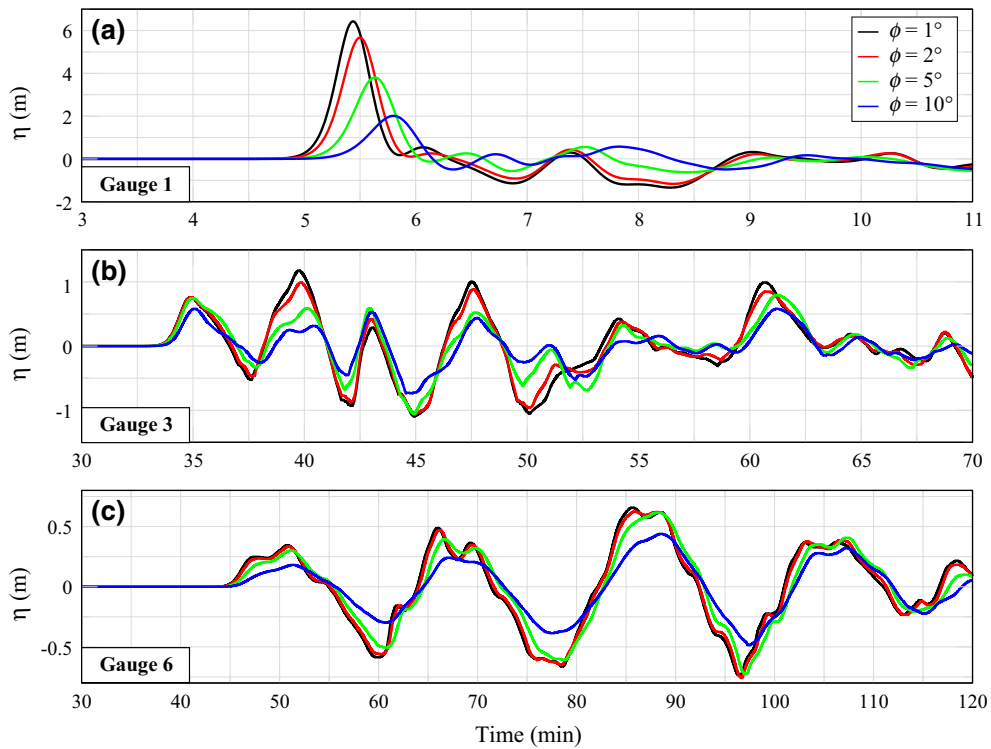


Figure 6

Time series calculated **a** at Gauge 1 near the Anak Krakatau volcano, **b** at Marina Jambu tide gauge (Gauge 3) and **c** at Kota Agung tide gauge (Gauge 6), using friction angles ϕ of 1° (black line), 2° (red line), 5° (green line) and 10° (blue line)

$$\begin{aligned} \frac{\partial v}{\partial t} + u \frac{\partial v}{\partial x} + v \frac{\partial v}{\partial y} &= -g \frac{\partial \eta}{\partial y} + \frac{d^3}{3} \left[\frac{\partial^2 v_t}{\partial y^2} + \frac{\partial^2 u_t}{\partial x \partial y} \right] \\ &+ \frac{d}{2} \left[v_t \frac{\partial^2 d}{\partial y^2} + v_t \frac{\partial^2 d}{\partial x \partial y} \right] + d \frac{\partial d}{\partial y} \frac{\partial v_t}{\partial y} \\ &+ \frac{d}{2} \left[\frac{\partial d}{\partial x} \frac{\partial u_t}{\partial y} + \frac{\partial d}{\partial y} \frac{\partial u_t}{\partial x} \right] + F_y \end{aligned} \quad (9)$$

where u_t and v_t the time-derivatives of u and v .

Both the landslide and shallow water equations, which are very similar, are solved by Godunov's finite-volume scheme, extended to second order by a Van Leer scheme (Heinrich et al. 2001a; Labb   et al. 2012). This numerical scheme was validated with an analytical solution in Mangeney et al. (2000). Boussinesq equations are solved using a finite-difference scheme for spatial derivatives together with a Crank–Nicolson scheme for the temporal discretization. This latter scheme is based on an iterative procedure that uses centered differences for linear terms and forward differences for advection terms. The implicit momentum equations are solved by alternating implicit sweeps in the x and y components using an ADI method (Alternating Direction Implicit). For a given direction, the dispersion terms in the other direction are discretized explicitly. For each direction (x and y), a tridiagonal matrix is then solved at each iteration, following Pedersen and L  vholt (2008).

The sea-bottom deformation due to the landslide, $\partial d / \partial t$ in Eq. (7), is computed as a forcing term:

$$\frac{\partial d}{\partial t} = \frac{1}{\cos \theta} \frac{\partial h_s}{\partial t} \quad (10)$$

4.3. Models Set-Up

For simulating the landslide and tsunami in the near-field (i.e. Anak Krakatau volcano and the other islands of the Krakatau archipelago), a pre-collapse topography and bathymetry of Gouhier and Paris (2019) was used. The pre-collapse topography of Anak Island was derived from the DEMNAS (national digital elevation model of Indonesia, spatial resolution of 0.27 arc-second using the vertical datum EGM2008, provided by the Indonesian Geospatial Agency, and available at <http://tides.big.go.id/DEMNAS/index.html>). The original DEMNAS was

slightly modified in order to include the latest growth of the edifice, as seen on photographs taken in August and November 2018,⁵ and satellite images (e.g. Sentinel-2 image captured on 30 September 2018, and PlanetScope image captured on 17 December 2018). Pre-collapse bathymetry is from Deplus et al. (1995). As explained in Gouhier and Paris (2019), the contour of the collapse scar was inferred from a Sentinel-1A image captured $\sim 8:30$ hours after the collapse (22/12/2018 at 22:33:44 UTC) and photographs taken by Susi Air flight crew the day after (23/12/2018).

Note that the subaerial volume estimated by Gouhier and Paris (2019) likely corresponds to a minimum value because there is no data available on post-collapse bathymetry and the submarine extent of the collapse scar. Considering a slope between 5 and 8° in the continuity of the subaerial landslide part, the total volume approaches 150 million m³. This volume is two times smaller than the volume of 270 million m³ modeled by Grilli et al. (2019). Pre and post-collapse topography and bathymetry around the Anak Krakatau are presented in Fig. 7c, d, respectively.

The bathymetric grids are built from the BAT-NAS one, with a spatial resolution of 180 m (available at <http://tides.big.go.id/DEMNAS/Batnas.php>). The model uses a system of multiple grids (coarse grid over deep water regions and fine grids over coastal regions) to model local effects of bathymetry. The parent nested grid covers the Sunda Strait, from eastern of Sumatra to western of Java Island (see Figs. 1 or 9 for the grid footprint). Five child grids are used with a resolution of approximately 25 m: the first domain covers the Kota Agung Bay, the second the Bandar Lampung Bay, the third the Kalianda area from northern of Taman Agung to southern of Lampung, the fourth the Teluk Lada area from western of Tanjung Lesung to southern of Anjer-Kidu, and the fifth the Anjer-Kidu area from Marina Jambu to eastern of Ciwandan (grids A, B, C, D and E, respectively, see Fig. 9).

⁵ <https://www.oysteinlundandersen.com/krakatau-volcano/krakatau-eruption-seen-from-panyer-west-java-17th-november-2018/>.

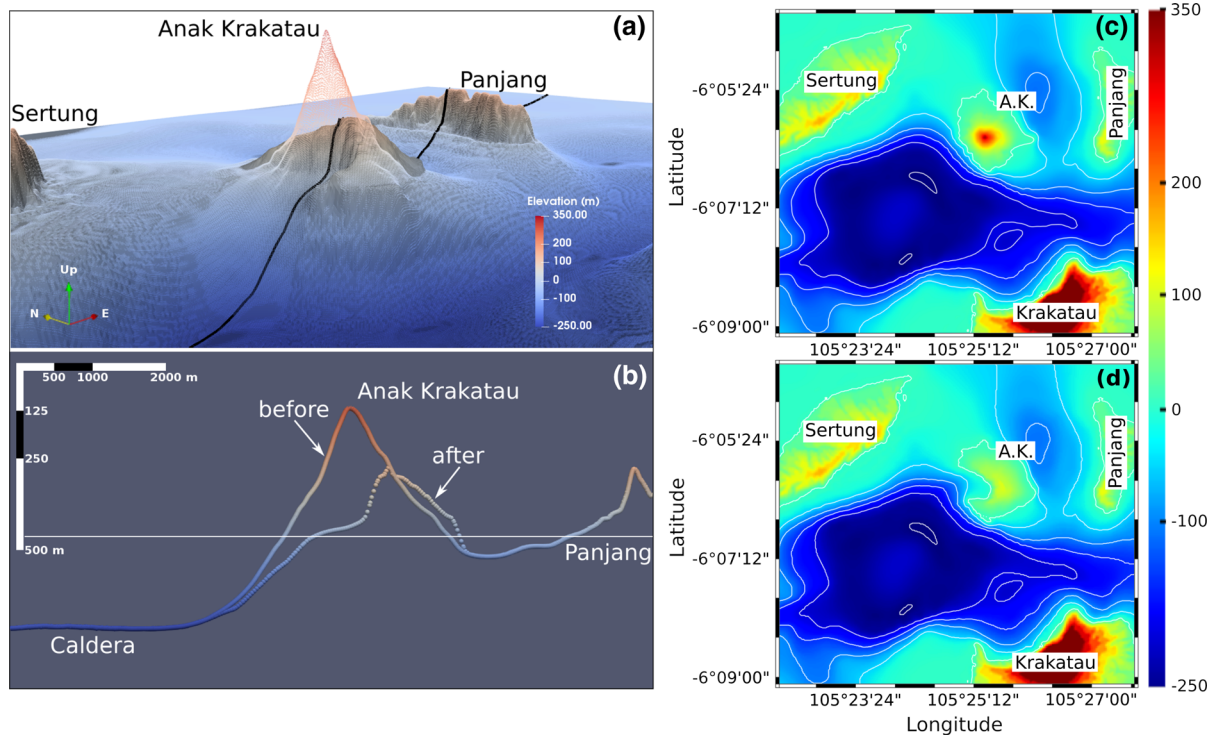


Figure 7

a Pre and post-collapse topo-bathymetry of Anak Krakatau volcano (dotted grid in transparency illustrating the pre-collapse volcanic edifice); **b** cross-section of the pre-collapse (solid line) and post-collapse (dotted line) topo-bathymetry following the black line in **a**. The water surface at rest is represented by the horizontal white line. There is a $\times 5$ vertical exaggeration. The scale in **a**, **b** is the same and only the view angle changes. Right panels show **c** pre and **d** post-collapse topo-bathymetry of Anak Krakatau volcano. Bathymetric contours range from 0 to -250 m every 50 m

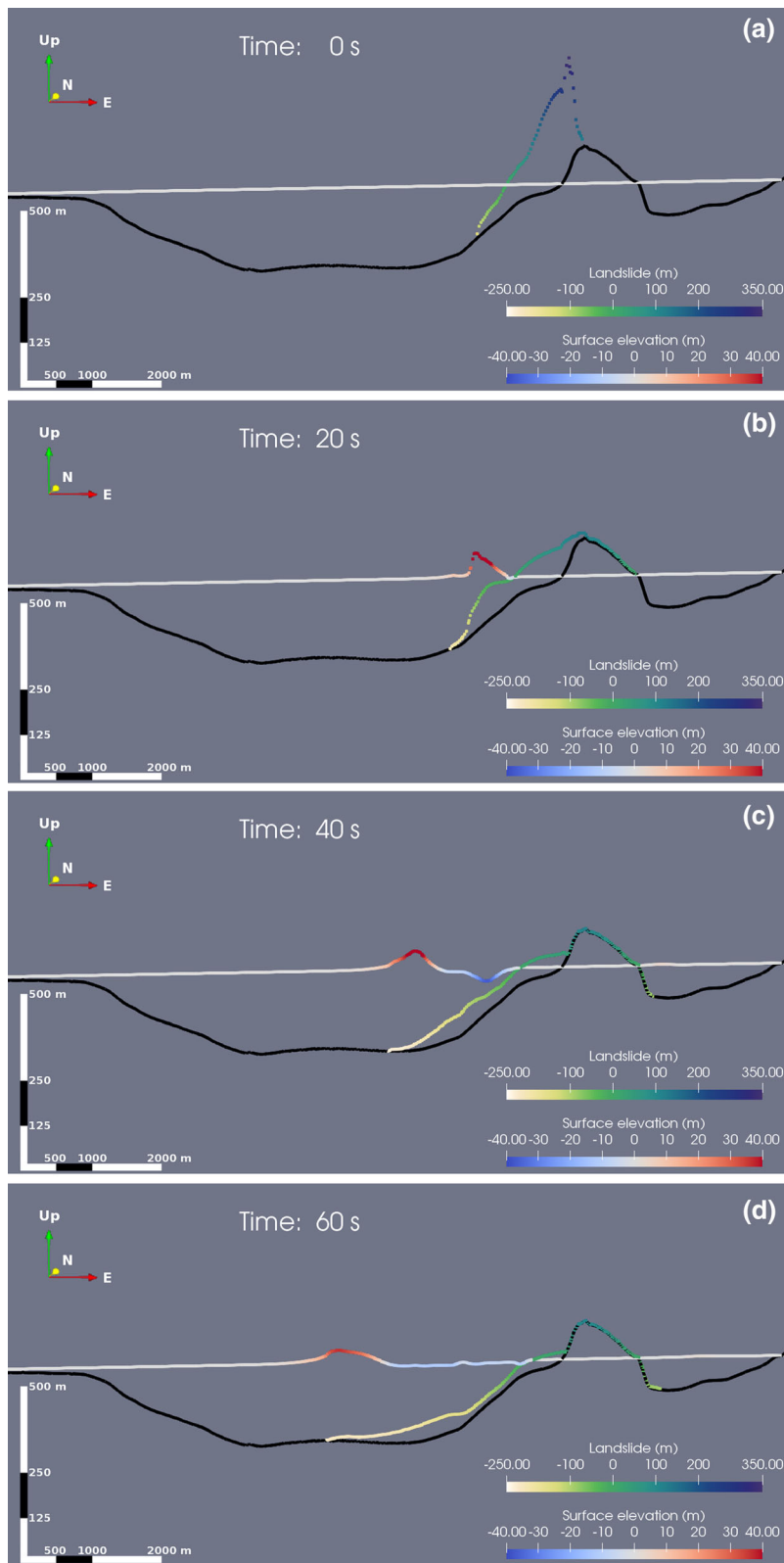
5. Results

5.1. Landslide Simulation

The sensitivity study realized on the basal friction angle shows that its influence on the generated wave heights decreases with distance. The basal friction angle plays a major role in the near-field (Gauge 1, Fig. 6a) but its influence is minor in the far-field (Gauges 3 and 6, Fig. 6b, c). There is no significant difference between 1 and 2° , at least in terms of computed wave height at the coasts. Using a friction angle of 2° , calculated water heights are of 75 cm at Marina Jambu and 33 cm at Kota Agung, whereas observed ones are of 60 and 35 cm, respectively. A friction angle of 10° results in wave heights of 56 and 16 cm respectively. Based on all the tide gauges, the best fit is obtained with a friction angle of 2° . This low value is consistent with the one used in Giachetti

et al. (2012) and other studies about landslides on volcanoes slopes [e.g. Le Friant et al. (2003) with 7° for the flank collapse of Montagne Pelée (Martinique, Lesser Antilles), Kelfoun et al. (2010) with values between 3 and 5° for different landslides scenarios envisaged at Reunion Island or Giachetti et al. (2011) with values between 1.3 and 3.9° for reproducing the Güímar debris avalanche (Tenerife, Canary Islands)].

A large part of the simulated landslide collapses in about 40 s (Fig. 8c), the volcano summit decreasing from about 350 m of altitude to about 120 m (Figs. 7, 8), which is concordant with the topographic reconstruction of Gouhier and Paris (2019). Beyond 40 s, the calculated ground displacement is negligible and no longer has any effect on the water surface deformation. The landslide covers a horizontal distance of about 4000 m from the volcano to the



◀Figure 8

Snapshots along a W–E cross-section of the simulated water wave (blue to red scale) and landslide (white to dark blue scale) at **a** $t = 0$ s, **b** $t = 20$ s, **c** $t = 40$ s and **d** $t = 60$ s. The post-collapse topography is represented in black solid line. There is a $\times 5$ vertical exaggeration

1883 submarine caldera, with an average velocity of 35 m.s^{-1} . Figure 7 shows both the numerical initial and final states of the volcano, with a cross-section illustrating the major topographic change induced by the flank collapse.

As shown by the temporal evolution of the landslide tip and the associated tsunami front (Fig. 8), velocities are quite similar, which can signify efficient transfer process. But further investigation may be needed as the part of the landslide with the largest thickness situated in smaller depth may be more important for energy transfer than the slide tip, and the wave is a bit too fast to stay in contact with this area.

5.2. Tsunami Simulation

Computed results are analyzed through a maximum surface elevations map (Fig. 9) covering the entire domain. On the tsunami path, synthetic gauges are located at places where tide gauges recorded the tsunami, i.e. Marina Jambu and Ciwandan for Java, Kota Agung and Panjang for Sumatra (Gauges 3, 4, 6 and 7 respectively, see Fig. 9, Table 1) and results are compared with detided data (the tide filter is based on the MATLAB package T_TIDE (Pawlowicz et al. 2002)) in Fig. 10. Other synthetic gauges are used, near the volcano, at Tanjung Lesung and Kalianda (Gauges 1, 2 and 5 respectively, see Fig. 9, Table 1) in order to compare the results to the field surveys data in these areas.

During the first 20 s of collapse the tsunami wave is being generated until it reaches a maximum positive elevation of 80 m (Fig. 8). Sertung Island is the first place to be hit after 80 s of wave propagation. It is located 3 km from the volcano which results in a wave celerity of about 38 m.s^{-1} . Rakata Island is hit in about the same time, with a

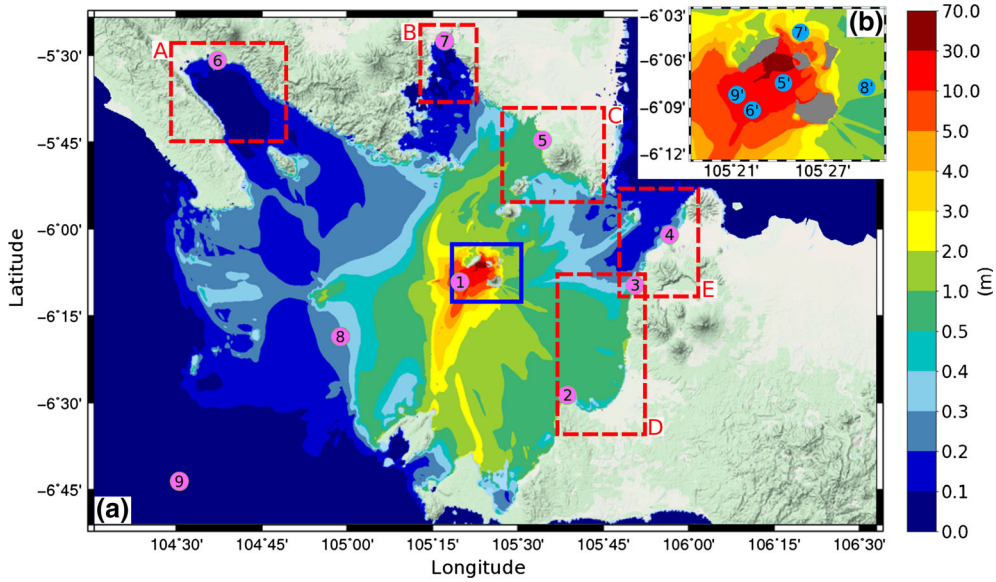


Figure 9

a Maximum surface elevations computed in Sunda Strait after the collapse of Anak Krakatau volcano. Pink discs with numbers represent the synthetic gauges locations: 10 km away from the volcano (1), at Tanjung Lesung (2), Marina Jambu (3), Ciwandan (4), Kalianda (5), Kota Agung (6), Panjang (7) and the two gauges (8 and 9) used for the comparison between the shallow water and the Boussinesq models. Child grids described in Sect. 4.3 are represented by the dashed red rectangles. **b** Close-up of the results around the volcano, corresponding to the blue box in **a**. Blue discs with numbers represent the synthetic gauges locations used by Grilli et al. (2019)

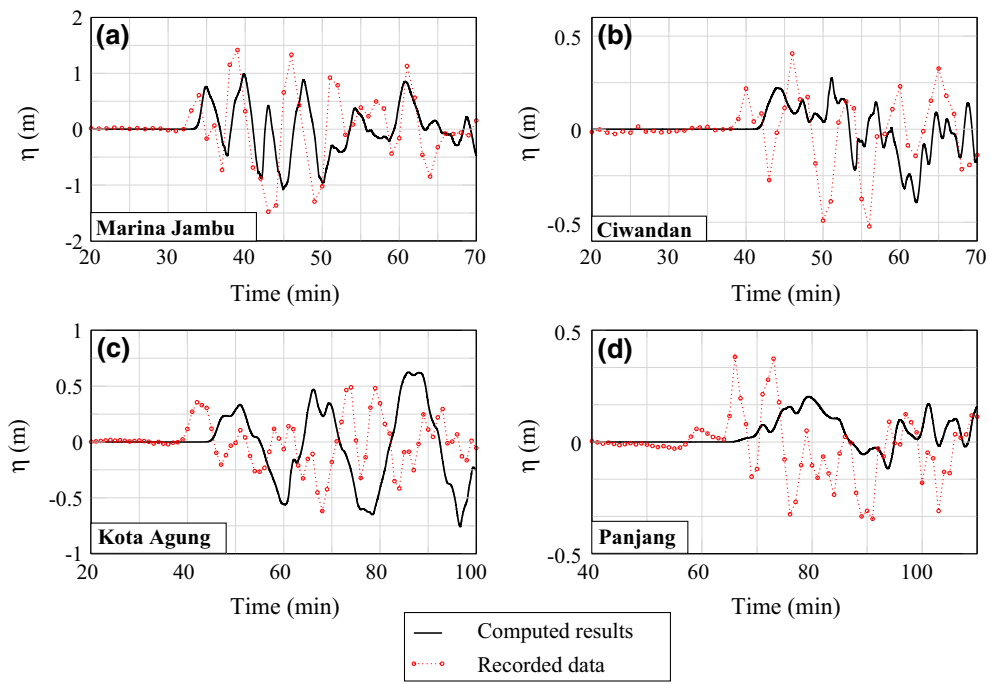


Figure 10

Comparison between recorded data (in red) and simulated water surface elevations (in black) at **a** Marina Jambu, **b** Ciwandan, **c** Kota Agung and **d** Panjang (Gauges 3, 4, 6 and 7, respectively, see Fig. 9)

speed of 50 m.s^{-1} . Then the wave travels around the Sunda Strait and reaches Gauge 1 [5 min after the collapse, with 5.6 m of wave height (Fig. 11a)], Gauge 2 [Tanjung Lesung, 29 min, 1.7 m (Fig. 11b)], Gauge 3 [Marina Jambu, 34 min, 75 cm (Fig. 10a)], Gauge 4 [Ciwandan, 42 min, 22 cm (Fig. 10b)], Gauge 5 [Kalianda, 49 min, 1.2 m (Fig. 11c)], Gauge 6 [Kota Agung, 45 min, 33 cm (Fig. 10c)] and Gauge 7 [Panjang, 1:06 hours, 20 cm (Fig. 10d)].

For the first wave, simulated water heights on the synthetic gauges are quite consistent with the tide gauges records (75 cm computed vs 60 cm recorded at Marina Jambu, 22 cm vs 20 cm at Ciwandan, 33 cm vs 35 cm at Kota Agung), excepted at Panjang (20 cm vs 37 cm). In addition, according to the concert video, the height of the first water wave is estimated to be 1–2 m, which is consistent with the computed water height of 1.7 m at Tanjung Lesung (Fig. 11b, Gauge 2). However, computed arrival times are late compared to the recorded ones (1 min at Marina Jambu, 3 min at Ciwandan, 5 min at Kota Agung and 8 min at Panjang). The general wave pattern is well

reproduced at Marina Jambu but poorly at Ciwandan, Kota Agung and Panjang.

5.3. Dispersion Assessment

In order to assess and highlight the potential dispersive effects in the Sunda Strait, shallow water simulation was performed with AVALANCHE and compared with the present Boussinesq simulation (Fig. 12). Time series calculated by the two models are compared at three synthetic gauges (Gauges 1, 8 and 9, Fig. 9) located in deep water at depths of 100 (Fig. 12a), 1140 (Fig. 12b) and 1960 m (Fig. 12c). Close to the source, both simulations produce approximately the same first water wave as depicted in Fig. 12a with water wave heights of about 5.5 m. However, dispersion effects are noticed in the far-field and in deep ocean. Compared to shallow water simulations, the period of the first wave increases during the propagation, ranging from about 1 min (Gauge 1, Fig. 12a) to about 1 min 30 s (Gauge 8, Fig. 12b) and about 2 min (Gauge 9, Fig. 12c).

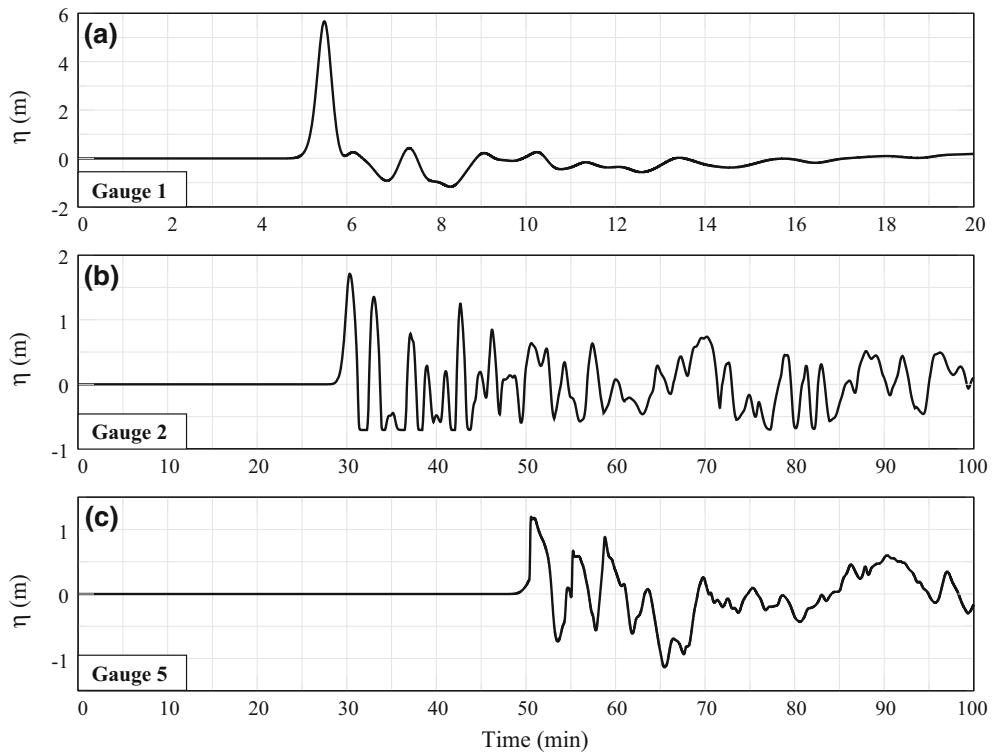


Figure 11
Computed surface elevations (m) **a** near the Anak Krakatau volcano, **b** at Tanjung Lesung and **c** at Kalianda (Gauges 1, 2 and 5, respectively, see Fig. 9)

6. Discussion

This study presents preliminary results of the 22 December 2018 Anak Krakatau collapse and tsunami simulations, comparing the computed numerical results with several observed data such as flow depths or recorded surface elevations. The main goal of this study was to better understand the landslide that occurred and assess its volume, despite the lack of submarine information. With the collapse of 150 million m³ modeled following a Coulomb frictional law, the obtained water heights are quite consistent with the observed ones, all over the Sunda Strait, and the computed amplitudes of the first wave match the tide gauges-extracted amplitudes (with errors ranging from 6% at Kota Agung to 25% at Marina Jambu), excepted at Panjang (error of 46%).

In comparison with the study of Grilli et al. (2019), our results (water heights and time delays of the first wave) are very similar at the four tide gauges,

with water heights differences of 50% at Marina Jambu, 12% at Ciwandan, 10% at Kota Agung and 0% at Panjang. In the near-field, our results are also very similar to the time series calculated at five additional gauges used by Grilli et al. (2019) (see Fig. 9b for gauges locations). The amplitudes of the generated water wave calculated by Grilli et al. (2019) are obviously larger in the near-field since the authors consider a landslide volume of 270 million m³. Nevertheless, we obtain the same arrival times, periods and to a lesser extent the same wave behaviour [see Fig. 13 in our paper and Figure 5 in Grilli et al. (2019)]. Our results are also similar in the near-field to those of Heidarzadeh et al. (2020). Considering a forward modeling trial-error approach, the latter ones obtain a wave height of about 100–150 m with a wavelength of 1.5–2 km. Their results are close to our first simulated wave characterized by a maximum amplitude of 80 m and a wavelength of

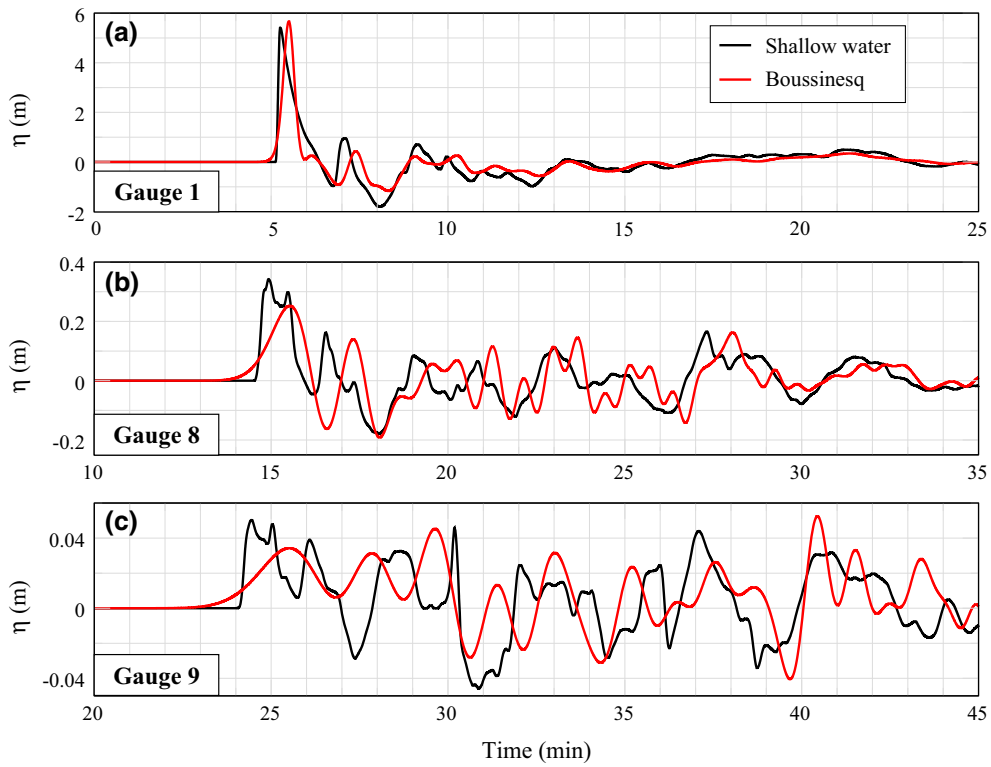


Figure 12

Comparison of time series calculated by the shallow water (in black) and the Boussinesq (in red) models at Gauges **a** 1, **b** 8 and **c** 9 (Fig. 9).

The water depths of these gauges are: **a** 100 m, **b** 1140 m and **c** 1960 m

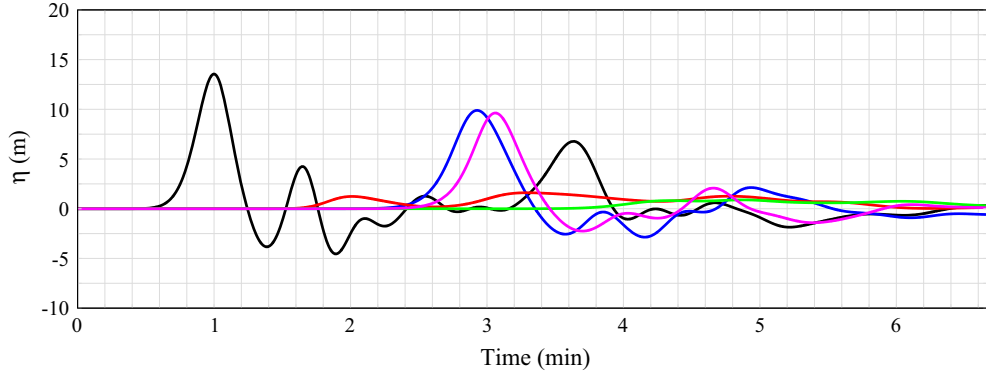


Figure 13

Time series of surface elevation calculated in the near-field by our model (150 million m³ and the code AVALANCHE) at the Gauges 5' (black), 6' (blue), 7' (red), 8' (green) and 9' (magenta) used by Grilli et al. (2019) and presented in Fig. 9b. Results are very similar to those presented in Figure 5e in Grilli et al. (2019)

about 2 km [see Fig. 8 in this study and Figure 12 in Heidarzadeh et al. (2020)].

Tables 2 and 3 show computed water heights at places studied by the field surveys of Takabatake

et al. (2019) and the BMKG, and the KKP, respectively. Although the comparison between inundation or run-up heights with water wave heights may be hard to realise, we see for instance that at Cipenuy

Beach, where highest run-up values were measured, we obtain the highest water heights. The computed wave heights are a little bit shorter than the observed ones by the BMKG survey, with 3–4 m vs 5–6 m. At the 5 locations close to the shoreline, i.e. distance lower than 30 m [Carita Lagon for BMKG survey (Table 2); Karang Suraga, Bulakan, Tanjung Jaya and Banyuasih for the KKP survey (Table 3)], the measured flow depths are on the same order that the computed tsunami height at the coast. Note that the bathymetric resolution (180 m interpolated to 25 m for the child grids) used in this study does not allow to compare precise inundation or run-up heights.

Although the results are encouraging, some limitations can be pointed out. First of all, the landslide reconstruction may be subject to discussion. It has been realized based on satellite images of the 23rd of December for the subaerial part and a quasi constant slope hypothesis for the submarine part. Unfortunately, the intense volcanic activity of the days following the tsunami has completely changed the shape of the volcano and it has made precise reconstruction impossible. Nevertheless, tsunami simulation associated to this landslide is rather consistent with observed water heights. A sensitivity study on the basal friction coefficient ϕ (Fig. 6) suggests that these water heights may vary quasi linearly with ϕ in the near-field, the smaller the friction angle, the higher the water wave heights. In the far-field along the coasts of Java or Sumatra, differences of water heights between $\phi = 1^\circ$ or $\phi = 2^\circ$ are not significant.

Second, the time delays of wave arrivals at the four tide gauges (Gauges 3, 4, 6 and 7, Fig. 9) could indicate that the landslide volume and its dynamics are unknown. However, sensitivity tests (not shown in this study) on the landslide volume produce similar results in terms of wave arrivals. In addition, our travel times are similar to those calculated by Giacchetti et al. (2012) and Grilli et al. (2019) for landslide volumes of 280 million m³ and 270 million m³, respectively. A possible explanation would be inaccuracies of the bathymetric data in this area. Travel times should thus be interpreted carefully. More information on the landslide will be available thanks to forthcoming surveys in the caldera.

Third, this study is a first attempt of simulating the collapse of Anak Krakatau volcano using 2D depth-averaged models both for the landslide and the tsunami. Several complex phenomena are not taken into account such as mixing of the slide with the surrounding water, soil erosion or dissipation of water waves due to wave breaking or friction.

Finally, according to Glimsdal et al. (2013), the dispersive effects can be estimated using the dispersion parameter:

$$\tau = \frac{4h_0^2L}{\lambda^3} \quad (11)$$

where h_0 is the depth at the source, L the distance to the coast of interest and λ the source width or in other terms the wavelength.

The dispersion parameter is ~ 1.4 at Kalianda up to ~ 3.4 at Kota Agung, with $h_0 = 250$ m, L between 45 and 110 km (see Table 1) and $\lambda = 2000$ m (see Fig. 8b), and suggests that the propagation is highly dispersive. Results of the comparison between the shallow water and Boussinesq simulations (Fig. 12) confirm that the first wave is subjected to dispersion, losing high-frequency components and being stretched by dispersive effects. After 25 min of propagation in deep ocean (Fig. 12c), the period is approximately two times longer and the amplitude decreases by about 50% compared to the one calculated by the shallow water model. The use of the Boussinesq model in this study is therefore relevant.

7. Conclusion

The 22 December, 2018 Anak Krakatau south-western flank collapse is modeled by a 2D depth-integrated code with a Coulomb frictional law and a basal friction angle of 2° . The generated tsunami is propagated using a Boussinesq model. This study highlighted some points and revealed some issues:

- The computed water heights from the present modeling fit well with those recorded at tide gauges of Marina Jambu, Ciwandan and Kota Agung (errors of 25%, 10% and 6%, respectively), with the video recorded at Tanjung Lesung and

- with the different observed data from the KKP, BMKG and Takabatake et al. (2019) field surveys.
- Results presented in this study are very similar to those obtained by Grilli et al. (2019) both in the near-field and in the far-field. However, their model is 3D, suggesting proper representation of the governing processes in both studies. Heights and wavelengths of the first wave are also very close to those obtained by Heidarzadeh et al. (2020) in the near-field.
 - Delays between simulated and observed travel times may be attributed to inaccuracies in the bathymetric data, particularly in the Bandar Lampung Bay.
 - Despite the lack of submarine information at the bottom of the volcano, the collapse of the reconstructed volume of 150 million m³ produces water waves that fit well with the observed results.
 - The sensitivity study on the basal friction angle shows that its influence on the generated wave heights decreases with distance and that there are no significant differences of water heights between basal friction coefficients of 1° or 2°.
 - Finally, a comparison between a Boussinesq model and a shallow water propagation highlights dispersive effects in the Sunda Strait that appear to be significant for the first waves. In deep waters, their periods progressively increase whereas their amplitudes progressively decrease.

Acknowledgements

We thank Abdul Muhari, from the Directorate of Sustainable Utilization of Coastal Zone and Small Islands, Ministry of Marine Affairs and Fisheries, Indonesia, for providing us with the tide gauges data and the KKP field survey data, and Gegar Prasetya, for providing us the BMKG field survey data.

Publisher's Note Springer Nature remains neutral with regard to jurisdictional claims in published maps and institutional affiliations.

REFERENCES

- Abadie, S., Harris, J., Grilli, S., & Fabre, R. (2012). Numerical modeling of tsunami waves generated by the flank collapse of the Cumbre Vieja Volcano (La Palma, Canary Islands): Tsunami source and near field effects. *Journal of Geophysical Research*, 117, 5.
- Assier-Rzadkiewicz, S., Heinrich, P., Sabatier, P., Savoye, B., & Bourillet, J. (2000). Numerical modelling of a landslide-generated tsunami: The 1979 Nice event. *Pure and Applied Geophysics*, 157(10), 1707–1727.
- Bondevik, S., Løvholt, F., Harbitz, C., Mangerud, J., Dawson, A., & Svendsen, J. (2005). The Storegga slide tsunami—comparing field observations with numerical simulations. *Marine and Petroleum Geology*, 22, 195–208.
- Camus, G., Gourgaud, A., & Vincent, P. (1987). Petrologic evolution of Krakatau (Indonesia): Implications for a future activity. *Journal of Volcanology and Geothermal Research*, 33, 299–316.
- Choi, B., Pelinovsky, E., Kim, K., & Lee, J. (2003). Simulation of the trans-oceanic tsunami propagation due to the 1883 Krakatau volcanic eruption, Copernicus Publications on behalf of the European Geosciences Union. *Natural Hazards and Earth System Science*, 3(5), 321–332.
- Cooke, R. (1981). Eruptive history of the volcano at Ritter Island. *Geological Survey of Papua New Guinea Memoir*, 10, 115–123.
- Deplus, C., Bonvalot, S., Dahrin, D., Diament, M., Harjono, H., & Dubois, J. (1995). Inner structure of the Krakatoa volcanic complex (Indonesia) from gravity and bathymetry data. *Journal of Volcanology and Geothermal Research*, 64, 23–51.
- Fine, I. V., Rabinovich, A. B., Thomson, R. E., & Kulikov, E. A. (2003). *Numerical modeling of tsunami generation by submarine and subaerial landslides* (pp. 69–88). Dordrecht: Springer.
- Franz, M., Jaboyedoff, M., Locat, J., & Podladchikov, Y. (2015). Testing a landslide-generated tsunami model. The case of the Nicolet landslide (Québec, Canada), In *Conference GEOQuébec 2015*, Québec City, QC, Canada.
- Fritz, H., Mohammed, F., & Yoo, J. (2009). Lituya Bay landslide impact generated mega-tsunami 50th anniversary. *Pure and Applied Geophysics*, 166, 153–175.
- Giachetti, T., Paris, R., Kelfoun, K., & Ontowirjo, B. (2012). Tsunami hazard related to a flank collapse of Anak Krakatau volcano, Sunda Strait, Indonesia. *Geological Society London Special Publication*, 361, 79–89.
- Giachetti, T., Paris, R., Kelfoun, K., & Pérez-Torrado, F. (2011). Numerical modelling of the tsunami triggered by the Güímar debris avalanche, Tenerife (Canary Islands): Comparison with field-based data. *Marine Geology*, 284, 189–202.
- Glimsdal, S., L'Heureux, J.-S., Harbitz, C., & Løvholt, F. (2016). The 29th January 2014 submarine landslide at Statland, Norway—landslide dynamics, tsunami generation, and run-up. *Landslides*, 13(6), 1435–1444.
- Glimsdal, S., Pedersen, G., Harbitz, C., & Løvholt, F. (2013). Dispersion of tsunamis: Does it really matter? *Natural Hazards and Earth System Sciences*, 13, 1507–1526.
- Gouhier, M., & Paris, R. (2019). SO₂ and tephra emissions during the December 22, 2018 Anak Krakatau flank-collapse eruption. *Volcanica*, 2(2), 91–103.
- Grilli, S., O'Reilly, C., Harris, J., Tajalli Bakhsh, T., Tehranirad, B., Banihashemi, S., et al. (2015). Modeling of SMF tsunami

- hazard along the upper US East Coast: Detailed impact around Ocean City, MD. *Natural Hazards*, 76, 705–746.
- Grilli, S., Tappin, D., Carey, S., Watt, S., Ward, S., Grilli, A., et al. (2019). Modelling of the tsunami from the December 22, 2018 lateral collapse of Anak Krakatau volcano in the Sunda Straits, Indonesia. *Scientific Reports*, 9, 11946.
- Grilli, S., & Watts, P. (2005). Tsunami generation by submarine mass failure. I: Modeling, experimental validation, and sensitivity analyses. *Journal of Waterway, Port, Coastal and Ocean Engineering*, 131(6), 283–297.
- Haflidason, H., Sejrup, H., Nygård, A., Meinert, J., Bryn, P., Lien, R., et al. (2004). The Storegga slide: Architecture, geometry and slide development. *Marine Geology*, 213(1–4), 201–234.
- Harbitz, C. (1992). Model simulations of tsunamis generated by the Storegga slides. *Marine Geology*, 105(1–4), 1–21.
- Harbitz, C., Glimsdal, S., Løvholt, F., Kveldsvik, V., Pedersen, G., & Jensen, A. (2014). Rockslide tsunamis in complex fjords: From an unstable rock slope at Åkerneset to tsunami risk in western Norway. *Coastal Engineering*, 88, 101–122.
- Harbitz, C., Pedersen, G., & Gjevik, B. (1993). Numerical simulations of large water waves due to landslides. *Journal of Hydraulic Engineering*, 119(12), 1325–1342.
- Harjono, H., Diament, M., Dubois, J., & Larue, M. (1991). Seismicity of the Sunda strait: Evidence for crustal extension and volcanological implications. *Tectonics*, 10, 17–30.
- Heidarzadeh, M., Ishibe, T., Sandanbata, O., Muhamri, A., & Wijanarto, A. (2020). Numerical modeling of the subaerial landslide source of the 22 December 2018 Anak Krakatoa volcanic tsunami Indonesia. *Ocean Engineering*, 20, 195.
- Heidarzadeh, M., Krastel, S., & Yalçiner, A. (2014). The state-of-the-art numerical tools for modeling landslide tsunamis: A short review. In S. Krastel, J.-H. Behrmann, D. Völker, M. Stipp, C. Berndt, R. Urgeles, J. Chaytor, K. Huhn, M. Strasser, & C. Harbitz (Eds.), *Submarine mass movements and their consequences: 6th international symposium* (pp. 483–495). Cham: Springer.
- Heinrich, P., Boudon, G., Komorowski, J. C., Sparks, R. S. J., Herd, R., & Voight, B. (2001b). Numerical simulation of the December 1997 Debris Avalanche in Montserrat, Lesser Antilles. *Geophysical Research Letters*, 28(13), 2529–2532.
- Heinrich, P., & Piatanesi, A. (2000). Near-field modeling of the July 17, 1998 tsunami in Papua New Guinea. *Geophysical Research Letters*, 27(19), 3037–3040.
- Heinrich, P., Piatanesi, A., & Hébert, H. (2001a). Numerical modelling of tsunami generation and propagation from submarine slumps: The 1998 Papua New Guinea event. *Geophysical Journal International*, 145(1), 97–111.
- Horrillo, J., Wood, A., Kim, G.-B., & Parambath, A. (2013). A simplified 3-D Navier-Stokes numerical model for landslide-tsunami: Application to the Gulf of Mexico. *Journal of Geophysical Research: Oceans*, 118(12), 6934–6950.
- Huang, B., Yin, Y., Wang, S., Tan, J., & Liu, G. (2017). Analysis of the Tangjiaxi landslide-generated waves in the Zhexi Reservoir, China, by a granular flow coupling model. *Natural Hazards and Earth System Sciences*, 17, 657–670.
- Hébert, H., Piatanesi, A., Heinrich, P., & Schindelé, F. (2002). Numerical modeling of the September 13, 1999 landslide and tsunami on Fatu Hiva Island (French Polynesia). *Geophysical Research Letters*, 29(10), 10–13.
- Jiang, L., & LeBlond, P. (1992). The coupling of a submarine slide and the surface waves which it generates. *Journal of Geophysical Research: Oceans*, 97(C8), 12731–12744.
- Johnson, R. (1987). Large-scale volcanic cone collapse; the 1888 slope failure of Ritter volcano. *Bulletin of Volcanology*, 49, 669–679.
- Kelfoun, K., Giachetti, T., & Labazuy, P. (2010). Landslide-generated tsunamis at Réunion Island. *Journal of Geophysical Research: Earth Surface*, 115, F4.
- Kirby, J., Shi, F., Nicolsky, D., & Misra, S. (2016). The 27 April 1975 Kitimat, British Columbia, submarine landslide tsunami: A comparison of modeling approaches. *Landslides*, 13, 1421–1434.
- Labbé, M., Donnadieu, C., Daubord, C., & Hébert, H. (2012). Refined numerical modeling of the 1979 tsunami in Nice (French Riviera): Comparison with coastal data. *Journal of Geophysical Research: Earth Surface*, 117, F1.
- Le Friant, A., Heinrich, P., Deplus, C., & Boudon, G. (2003). Numerical simulation of the last flank-collapse event of Montagne Pelée, Martinique, Lesser Antilles. *Geophysical Research Letters*, 30, 2.
- L'Heureux, J.-S., Glimsdal, S., Longva, O., Hansen, L., & Harbitz, C. (2011). The 1888 shoreline landslide and tsunami in Trondheimsfjorden, central Norway. *Marine Geophysical Research*, 32(1), 313–329.
- Liu, P.-F., Woo, S.-B., & Cho, Y.-S. (1998). *Computer programs for tsunami propagation and inundation* (p. 25). Cornell: Cornell University.
- Løvholt, F., Pedersen, G., & Gisler, G. (2008). Oceanic propagation of a potential tsunami from the La Palma Island. *Journal of Geophysical Research: Oceans*, 113(9), 1–21.
- Ma, G., Kirby, J., Hsu, T.-J., & Shi, F. (2015). A two-layer granular landslide model for tsunami wave generation: Theory and computation. *Ocean Modelling*, 93, 40–55.
- Ma, G., Shi, F., & Kirby, J. (2012). Shock-capturing non-hydrostatic model for fully dispersive surface wave processes. *Ocean Modelling*, 43–44, 22–35.
- Mangeney, A., Heinrich, P., & Roche, R. (2000). Analytical solution for testing debris avalanche numerical models. *Pure and Applied Geophysics*, 157, 1081–1096.
- Masson, D., Harbitz, C., Wynn, R., Pedersen, G., & Løvholt, F. (2006). Submarine landslides: Processes, triggers and hazard prediction. *Philosophical Transactions of the Royal Society A: Mathematical, Physical and Engineering Sciences*, 364(1845), 2009–2039.
- Miller, D. J. (1960). Giant waves in Lituya Bay, Alaska. *US Geological Survey Professional Paper*, 354-C.
- Muhamri, A., Heidarzadeh, M., Susmoro, H., Nugroho, H., Kriswati, E., Supartoyo, W. A., et al. (2019). The December 2018 Anak Krakatau Volcano tsunami as inferred from post-tsunami field surveys and spectral analysis. *Pure and Applied Geophysics*, 21, 1–5.
- Nishimura, S., Nishida, J., Yokoyama, T., & Hehuwat, F. (1986). Neotectonics of the Straits of Sunda, Indonesia. *Journal of Southeast Asian Earth Science*, 1, 81–91.
- Nomanbhoy, N., & Satake, K. (1995). Generation mechanism of tsunamis from the 1883 Krakatau eruption. *Geophysical Research Letters*, 22(4), 509–512.
- Okal, E. A., & Synolakis, C. E. (2003). A theoretical comparison of tsunamis from dislocations and landslides. *Pure and Applied Geophysics*, 160(10–11), 2177–2188.

- Paris, A., Okal, E., Guérin, C., Heinrich, P., Schindelé, F., & Hébert, H. (2019). Numerical modeling of the June 17, 2017 landslide and tsunami events in Karrat Fjord, west Greenland. *Pure and Applied Geophysics*, 176(7), 3035–3057.
- Pawlowicz, R., Beardsley, B., & Lentz, S. (2002). Classical tidal harmonic analysis including error estimates in MATLAB using T\TIDE. *Computers and Geosciences*, 28, 929–937.
- Pedersen, G. & Løvholt, F. (2008). Documentation of a global Boussinesq solver. *Preprint series in Applied Mathematics 1. <http://urn.nb.no/URN:NBN:no-27775>*.
- Poupardin, A., Heinrich, P., Frère, A., Imbert, D., Hébert, H., & Flouzat, M. (2017). The 1979 submarine landslide-generated tsunami in Mururoa, French Polynesia. *Pure and Applied Geophysics*, 174, 3293–3311.
- Rodriguez, M., Chamot-Rooke, N., Hébert, H., Fournier, M., & Huchon, P. (2013). Owen Ridge deep-water submarine landslides: Implications for tsunami hazard along the Oman coast. *Natural Hazards and Earth System Science*, 13, 417–424.
- Satake, K., & Kato, Y. (2001). The 1741 Oshima–Oshima eruption: Extent and volume of submarine debris avalanche. *Geophysical Research Letters*, 28, 427–430.
- Satake, K., Smith, J., & Shinozaki, K. (2002). *'Three-dimensional reconstruction and tsunami model of the Nuuanu and Wailau giant landslides* (pp. 333–346). Hawaii: American Geophysical Union Geophysical Monograph Series.
- Savage, S. B., & Hutter, K. (1989). The motion of a finite mass of granular material down a rough incline. *Journal of Fluid Mechanics*, 199, 177–215.
- Savage, S. B., & Hutter, K. (1991). The dynamics of avalanches of granular materials from initiation to runout. Part I: Analysis. *Acta Mechanica*, 86(1), 201–223.
- Shi, F., Kirby, J., Harris, J., Geiman, J., & Grilli, S. (2012). A high-order adaptive time-stepping TVD solver for Boussinesq modeling of breaking waves and coastal inundation. *Ocean Modelling*, 43–44, 36–51.
- Sigurdsson, H., Carey, S., Mandeville, C., & Bronto, S. (1991). Pyroclastic flows of the 1883 Krakatau eruption. *Eos Transactions of the American Geophysical Union*, 72(36), 377–392.
- Simkin, T., & Fiske, R. (1983). *Krakatau 1883: The volcanic eruption and its effects*. Washington, D.C.: Smithsonian Institution Press.
- Skvortsov, A., & Bornhold, B. (2007). Numerical simulation of the landslide-generated tsunami in Kitimat Arm, British Columbia, Canada, 27 April 1975. *Journal of Geophysical Research: Earth Surface*, 112, 2.
- Stehn, C. (1929). The geology and volcanism of the Krakatau Group. In *Proceedings of the Fourth Pacific science congress*, pp. 1–55.
- Sudradjat, A. (1982). The morphological development of Anak Krakatau Volcano, Sunda Strait. *Geologi Indonesia*, 9, 1–11.
- Susilohadi, S., Gaedicke, C., & Djajadihardja, D. (2009). Structures and sedimentary deposition in the Sunda Strait, Indonesia. *Tectonophysics*, 467, 55–71.
- Synolakis, C. E., Bardet, J.-P., Borrero, J. C., Davies, H. L., Okal, E. A., Silver, E. A., Sweet, S., & Tappin, D. R. (2002). The slump origin of the 1998 Papua New Guinea tsunami. In *Proceedings of the Royal Society of London, series A: Mathematical, physical and engineering sciences*, Vol. 458, The Royal Society, pp. 763–789.
- Takabatake, T., Shibayama, T., Esteban, M., Achiari, H., Nurisman, N., Gelfi, M., et al. (2019). Field survey and evacuation behaviour during the 2018 Sunda Strait tsunami. *Coastal Engineering Journal*, 20, 1–21.
- Tappin, D., Grilli, S., Harris, J., Geller, R., Masterlark, T., Kirby, J., et al. (2014). Did a submarine landslide contribute to the 2011 Tohoku tsunami? *Marine Geology*, 357, 344–361.
- Tappin, D., Watts, P., & Grilli, S. (2008). The Papua New Guinea tsunami of 17 July 1998: Anatomy of a catastrophic event. *Natural Hazards and Earth System Sciences*, 8, 243–266.
- TDmRC (2019) The latest update from post-Sunda Strait tsunami survey. <http://tdmrc.unsyiah.ac.id/the-latest-update-from-post-sunda-strait-tsunami-survey/>.
- Walter, T., Haghghi, M., Schneider, F., Coppola, D., Motagh, M., Saul, J., Babeyko, A., Dahm, T., Troll, V., Tilmann, F., Heimann, S., Valade, S., Triyono, R., Khomarudin, R., Kartadinata, N., Laiolo, M., Massimetti, F., & Gaebler, P. (2019). Precursors and processes culminating in the Anak Krakatau December 2018 sector collapse and tsunami. *Nature Communications*(in revision).
- Wang, X., & Liu, P.-F. (2006). An analysis of 2004 Sumatra earthquake fault plane mechanisms and Indian Ocean tsunami. *Journal of Hydraulic Research*, 44, 147–154.
- Yavari-Ramshe, S., & Ataie-Ashtiani, B. (2016). Numerical modeling of subaerial and submarine landslide-generated tsunami waves—recent advances and future challenges. *Landslides*, 13, 1325–1368.

(Received September 13, 2019, revised December 8, 2019, accepted December 11, 2019, Published online December 20, 2019)

Terms and Conditions

Springer Nature journal content, brought to you courtesy of Springer Nature Customer Service Center GmbH (“Springer Nature”). Springer Nature supports a reasonable amount of sharing of research papers by authors, subscribers and authorised users (“Users”), for small-scale personal, non-commercial use provided that all copyright, trade and service marks and other proprietary notices are maintained. By accessing, sharing, receiving or otherwise using the Springer Nature journal content you agree to these terms of use (“Terms”). For these purposes, Springer Nature considers academic use (by researchers and students) to be non-commercial.

These Terms are supplementary and will apply in addition to any applicable website terms and conditions, a relevant site licence or a personal subscription. These Terms will prevail over any conflict or ambiguity with regards to the relevant terms, a site licence or a personal subscription (to the extent of the conflict or ambiguity only). For Creative Commons-licensed articles, the terms of the Creative Commons license used will apply.

We collect and use personal data to provide access to the Springer Nature journal content. We may also use these personal data internally within ResearchGate and Springer Nature and as agreed share it, in an anonymised way, for purposes of tracking, analysis and reporting. We will not otherwise disclose your personal data outside the ResearchGate or the Springer Nature group of companies unless we have your permission as detailed in the Privacy Policy.

While Users may use the Springer Nature journal content for small scale, personal non-commercial use, it is important to note that Users may not:

1. use such content for the purpose of providing other users with access on a regular or large scale basis or as a means to circumvent access control;
2. use such content where to do so would be considered a criminal or statutory offence in any jurisdiction, or gives rise to civil liability, or is otherwise unlawful;
3. falsely or misleadingly imply or suggest endorsement, approval , sponsorship, or association unless explicitly agreed to by Springer Nature in writing;
4. use bots or other automated methods to access the content or redirect messages
5. override any security feature or exclusionary protocol; or
6. share the content in order to create substitute for Springer Nature products or services or a systematic database of Springer Nature journal content.

In line with the restriction against commercial use, Springer Nature does not permit the creation of a product or service that creates revenue, royalties, rent or income from our content or its inclusion as part of a paid for service or for other commercial gain. Springer Nature journal content cannot be used for inter-library loans and librarians may not upload Springer Nature journal content on a large scale into their, or any other, institutional repository.

These terms of use are reviewed regularly and may be amended at any time. Springer Nature is not obligated to publish any information or content on this website and may remove it or features or functionality at our sole discretion, at any time with or without notice. Springer Nature may revoke this licence to you at any time and remove access to any copies of the Springer Nature journal content which have been saved.

To the fullest extent permitted by law, Springer Nature makes no warranties, representations or guarantees to Users, either express or implied with respect to the Springer nature journal content and all parties disclaim and waive any implied warranties or warranties imposed by law, including merchantability or fitness for any particular purpose.

Please note that these rights do not automatically extend to content, data or other material published by Springer Nature that may be licensed from third parties.

If you would like to use or distribute our Springer Nature journal content to a wider audience or on a regular basis or in any other manner not expressly permitted by these Terms, please contact Springer Nature at

onlineservice@springernature.com